MOLECULAR AND CELLULAR BIOLOGY, Oct. 2007, p. 6794–6805 Vol. 27, No. 19
0270-7306/07/$08.00+0 doi:10.1128/MCB.01029-07

Loss of Zona Pellucida Binding Proteins in the Acrosomal Matrix Disrupts Acrosome Biogenesis and Sperm Morphogenesis▽†

Yi-Nan Lin,[1,2] Angshumoy Roy,[1,3] Wei Yan,[1]‡ Kathleen H. Burns,[1,3]§ and Martin M. Matzuk[1,2,3]*

Departments of Pathology,[1] Molecular and Cellular Biology,[2] and Molecular and Human Genetics,[3] Baylor College of Medicine, Houston, Texas 77030

Received 11 June 2007/Returned for modification 26 June 2007/Accepted 18 July 2007

Zona pellucida binding protein 1 (ZPBP1), a spermatid and spermatozoon protein that localizes to the acrosome, was originally identified in pigs and named for its binding to the oocyte zona pellucida. In an in silico search for germ cell-specific genes, *Zpbp1* and its novel paralog, *Zpbp2*, were discovered and confirmed to be expressed only in the testes in both mice and humans. To study the in vivo functions of both ZPBP proteins, we disrupted *Zpbp1* and *Zpbp2* in mice. Males lacking ZPBP1 were sterile, with abnormal round-headed sperm morphology and no forward sperm motility. Ultrastructural studies demonstrated that absence of ZPBP1 prevents proper acrosome compaction, resulting in acrosome fragmentation and disruption of the Sertoli-spermatid junctions. Males null for ZPBP2 were subfertile, demonstrated aberrant acrosomal membrane invaginations, and produced dysmorphic sperm with reduced ability to penetrate zona pellucida. Molecular phylogenetic analysis of *ZPBPs* from amphibians, birds, and mammals suggests that these paralogous genes coevolved to play cooperative roles during spermiogenesis. Whereas ZPBP1 was discovered for an in vitro role in sperm-egg interactions, we have shown that both ZPBP proteins play an earlier structural role during spermiogenesis.

Studies on sperm-egg interactions in model organisms have provided conceptual understandings for how spermatozoa bind, penetrate, and fertilize the egg (15, 49). In placental mammals (Eutheria), the egg investment, called the zona pellucida (ZP), is a reticular meshwork assembled from three groups of sulfated glycoproteins, ZP2, ZP3, and ZP1/ZP4 that completely encircles mammalian eggs (12, 15). The ZP is responsible for the initial sperm binding and the subsequent induction of the acrosome reaction that allows sperm penetration. The ZP also functions as a physical barrier to select for functional spermatozoa capable of successful penetration, to prevent polyspermy, and to protect early embryos. However, the molecular details of sperm binding and zona penetration are mostly unresolved (36). Therefore, much effort has been focused on identifying sperm proteins involved in these processes.

The acrosome is a cap-shaped, Golgi-derived organelle located over the anterior part of the sperm nucleus and highly conserved throughout evolution (2, 13). One exception in vertebrates is the teleost (bony fish) lineage, in which acrosomeless sperm can fertilize the egg by swimming through a specialized opening on the egg investment known as the micropyle (10, 32). During the acrosome reaction, the vesiculization and removal of the sperm plasma membrane and the outer acrosomal membrane expose the inner acrosomal membrane and the overlaying acrosomal matrix materials for subsequent sperm-egg interactions, including zona penetration and sperm-egg fusion (15, 16, 49). Although acrosome biogenesis is important for sperm during gamete interaction, recent studies have also revealed its involvement in sperm morphogenesis (21). During spermiogenesis, close association of the acrosome with the underlying nucleus through the acroplaxome (20) is likely involved in the formation and maintenance of nuclear polarity in spermatids during chromatin condensation through chromatin components such as H1T2 (26). The acrosome also anchors the spermatid nucleus to the Sertoli cell through Sertoli-spermatid junctions, including the apical ectoplasmic specializations until the time of spermiation (47).

During our in silico subtraction studies to identify novel germ-cell-specific genes in the mouse (24, 37), we found ZP binding protein 1 (*Sp38*) (30, 31) or *Iam38* (51) (herein referred to as *Zpbp1*) and its novel paralog, *Zpbp2*. ZPBP1 has been previously identified as an in vitro ZP2(ZPA)-binding protein (30) associated with the persistent acrosomal matrix over the inner acrosomal membrane of acrosome-reacted sperm (31, 51); an anti-ZPBP1 antibody has also been shown to block in vitro fertilization in pigs, potentially acting at the zona penetration step (51).

Here, we report the identification of members of the *ZPBP* gene family from amphibians to mammals and the physiological characterization of both ZPBP1 and ZPBP2 using knockout mouse models. Unexpectedly and in contrast to the reported in vitro roles of ZPBPs in fertilization, we uncovered in vivo structural functions for both ZPBP proteins in the biogenesis of the acrosome and sperm morphogenesis during spermiogenesis. Implications of the overlapping, but different, localizations of ZPBP1 and ZPBP2 in the acrosomal matrix, their different biochemical properties, possible coevolutionary relationships between the ZPBPs, and mechanisms of sperm-egg interaction are discussed.

* Corresponding author. Mailing address: Department of Pathology, Baylor College of Medicine, One Baylor Plaza, Houston, TX 77030. Phone: (713) 798-6451. Fax: (713) 798-5833. E-mail: mmatzuk@bcm.tmc.edu.

† Supplemental material for this article may be found at http://mcb.asm.org/.

‡ Present address: Department of Physiology and Cell Biology, University of Nevada School of Medicine, Reno, NV 89557.

§ Present address: Department of Pathology, Johns Hopkins School of Medicine, Baltimore, MD 21287.

▽ Published ahead of print on 30 July 2007.

MATERIALS AND METHODS

In silico subtraction and semiquantitative RT-PCR. In silico subtraction was performed as described earlier (39). The identified genes were further screened for tissue specificity by using semiquantitative reverse transcription-PCR (RT-PCR) as described previously (48). Primers were designed to span exons. Mouse cDNAs were prepared from multiple mouse tissues, and human multiple tissue cDNAs were purchased from BD Biosciences. The following gene-specific primers were used: mouse *Zpbp1*, TTGGACATTTGGCTCGACTG and AGCTGC ATGGTATCGAGCTG; mouse *Zpbp2*, ACTAGTGCCTGAGCCGTGAT and AGGTTCCCGATATGCAAAGA; human *ZPBP1*, CAAAGAGCTGGTTTGC AAAATG and AAGCACGTTTTTGCTCCATACA; and human *ZPBP2*, TTG GAGCCTTTGTCTGGACT and ATATGCTTGGCTCCGAAAAA. Human β-actin was amplified as a loading control by using a primer set purchased from BD Biosciences. To ensure that the PCR was in the exponential phase, different PCR cycles from 15 to 35 were tested. Twenty-eight cycles were used for both mouse *Zpbp2* and human *ZPBP2.* The mouse *Hprt1* and human β-*ACTIN* served as loading controls for the PCRs.

Genomic database search and protein sequence alignment. The amino acid sequences from the open reading frames of mouse *Zpbp1* and *Zpbp2* sequence were used to perform a TBLASTN search against the different GenBank database subsets, including the nonredundant database, the EST database, and the WGS database as described by Roy et al. (38). Reciprocal best matches were used as criteria to verify the orthologous pairs. An alignment of all ZPBP proteins of different species was performed by using the MEGALIGN program of the DNASTAR software package (DNASTAR, Inc.). The sequence similarity was derived by using the same program.

5′RACE. To verify the completeness at the 5′ end, rapid amplification of cDNA 5′ ends (5′RACE) was performed by using a SMART RACE cDNA amplification kit (BD Biosciences) according to the manufacturer's instructions. The amplified DNA fragments visible on an ethidium bromide gel were isolated and cloned into pGEM-T vector (Promega) for subsequent sequencing.

In situ hybridization. In situ hybridization was performed as described previously (48). Briefly, paraffin-embedded testes were cut into 5-μm sections, dewaxed, fixed, hybridized, and washed. The mouse *Zpbp1* cDNA fragment (nucleotides 31 to 1245 in NM_015785) and the mouse *Zpbp2* cDNA fragment (nucleotides 105 to 539 in AY251601) were cloned into pGEM-T vector. Sense and antisense probes were generated by labeling with [α-^{35}S]uridine phosphate by using the Riboprobe labeling system (Promega). Hybridization signals were detected by autoradiography using NTB-2 emulsion (Eastman Kodak). After development and fixation, the slides were counterstained with hematoxylin and mounted for photography. Neither the mouse *Zpbp1* nor the *Zpbp2* sense probes generated a signal above the background in the testes sections.

Generation of anti-ZPBP1 and anti-ZPBP2 antibodies. Recombinant mouse *Zpbp1* (amino acids 101 to 406 in NP_056600), produced from the pET-23b(+) vector (Novagen), was used to immunize goats (Cocalico Biologicals) to produce the anti-ZPBP1 polyclonal antibody (G176). A mouse ZPBP2 peptide (KETV DPTYLWTGPNE; amino acids 62 to 76 in NP_081337) was used to generate affinity-purified anti-ZPBP2 antibody in rabbit (Bethyl Laboratories).

Immunofluorescence microscopy. Immunofluorescence microscopy was performed on tubule squash preparations as described previously (22) or on air-dried epididymal sperm. Briefly, seminiferous tubules were dissected and staged before squashing. The tubule squash preparations were fixed in 90% ethanol for immunofluorescence labeling, and epididymal sperm were permeabilized with 0.5% Triton X-100 in phosphate-buffered saline (PBS) and fixed with 3:1 methanol-acetic acid. The goat anti-ZPBP1 polyclonal antibody (G176) was used at a dilution of 1:200, and the rabbit anti-ZPBP2 peptide antibody was used at a dilution of 1:2,000. Secondary antibodies conjugated with Alexa fluorochrome (Invitrogen) were used to visualize protein localizations. Negative controls, omitting the primary antibodies, showed only background signals.

Generation of *Zpbp1* and *Zpbp2* knockout mice. The targeting constructs were electroporated into *Hprt*-deficient AB2.2 mouse embryonic stem (ES) cells derived from a 129S5/SvEvBrd (129S5) strain, and double selection was used to screen for targeted clones as described previously (27). Proper targeting was verified by Southern blot analysis with both 5′ and 3′ probes. Two different ES cell clones carrying targeted *Zpbp2* allele and one ES cell clone carrying targeted *Zpbp1* allele were injected into recipient C57BL/6J blastocysts to generate chimeric mice. The examination of another gene, AK040906, whose exon 1 is localized in the 5′-recombination arm, but unknown at the time of vector construction, involved semiquantitative RT-PCR, 5′RACE, and sequencing of cloned cDNA to rule out mutations in this gene. Chimeric males were bred to females of both the C57BL/6J (B6) and 129S5 strains to obtain F_1 heterozygous mice carrying targeted mutant alleles. Male and female F_1 heterozygotes were intercrossed to produce homozygous mutant mice. Male and female progeny were born with the expected Mendelian frequency at approximately 1:1 ratio for both sexes. All mouse experiments were carried out on a C57BL/6/129S5/SvEvBrd hybrid background. Litters were weaned at 3 weeks, and mice were mated at 42 days. The number of litters and pups per litter born over a 6-month period were recorded to obtain the mean litter sizes and the average litters born in 6 months. All animal experiments were performed in accordance with protocols approved by the Institutional Animal Care and Use Committee of Baylor College of Medicine.

Northern blot analysis. Total RNA (15 μg) isolated from multiple mouse tissues was fractionated on a 1.2% formaldehyde-agarose gel and transferred to Hybond-N nylon membrane (GE Healthcare). The 697-bp (nucleotides 405 to 1101 in NM_015785) fragment of mouse *Zpbp1* cDNA and 721-bp (nucleotides 336 to 1056 in NM_027061) fragment of mouse *Zpbp2* cDNA was labeled with [α-^{32}P]deoxy(d)-ATP using the Strip-EZ kit (Ambion). Membrane hybridization, washing, and autoradiography, as well as stripping and reprobing, were performed according to the manufacturer's instructions. Blots were stripped and hybridized with a *Gapdh* cDNA labeled with [α-^{32}P]dATP to verify equal RNA loading.

Sperm parameter analysis. Caudal spermatozoa from adult mice were prepared by mincing caudal epididymides in prewarmed M2 medium, and sperm were allowed to swim out by incubation at 37°C under 5% CO_2 in air for 30 min. For sperm counts, sperm are immobilized by dilution in water and counted with a hemacytometer in duplicate to obtain an average. For analysis of percent motility, 15 μl of an aliquot of sperm diluted to 10^6/ml was spotted onto a glass slide and covered with a 22-by-22-mm coverslip. A total of 100 sperm (both motile and immotile) were scored in duplicate manually using differential interference contrast optics at ×200 to obtain an average percent motility.

Electron microscopy. For transmission electron microscopy analysis, epididymis or testes from transcardially perfused mice were further fixed in 2.5% glutaraldehyde and 2.0% formaldehyde in 0.1 M cacodylate buffer containing 2 mM $CaCl_2$ and embedded in Spurr's resin. Thin sections (80 nm) were made and stained with uranyl acetate and lead citrate, and electron microscopy was performed using a Hitachi H7500 transmission electron microscope (Hitachi-HTA) at 80 kV.

Monitoring in vivo fertilized embryos. The collection of in vivo fertilized two-pronucleus embryos were performed as described by Nagy (33). Briefly, superovulation is performed with intraperitoneal injections of 5 IU of pregnant mare serum gonadotropin, followed 48 h later with 5 IU of human chorionic gonadotropin (hCG). Female C57/129S5 mice, 2 to 3 months old, were superovulated and mated to *Zpbp2* heterozygous or *Zpbp2*-null males. Test females were checked for vaginal plugs the next morning and sacrificed for embryo collection 24 h after the injection of hCG. After DNA was stained with DAPI (4′,6′-diamidino-2-phenylindole), the percentages of embryos with two pronuclei were recorded.

In vitro sperm-egg binding with zona-intact eggs and fusion assay with zona-free eggs. The in vitro sperm-egg binding assay was performed as described previously (46). Briefly, superovulated eggs were treated with hyaluronidase in M199* (M199 medium [Invitrogen] supplemented with 30 μg of sodium pyruvate/ml) to remove cumulus cells, washed in PBS-PVP (PBS with 0.4% polyvinylpyrrolidone), and fixed in 1% formaldehyde–PBS-PVP for use up to 1 week. Fixed eggs were washed three times for 20 min each in M199* plus 0.4% bovine serum albumin (M199*+0.4% BSA) before use. Caudal epididymal sperm were capacitated in M199*+0.4% BSA for 1 h at 37°C in 5% CO_2 and adjusted to a concentration of 10^5/ml. Twelve eggs were added for each assay. After an incubation period of 50 min, eggs were washed in M199*+0.4% BSA and fixed in 2% formaldehyde–PBS-PVP, and the number of bound sperm per egg was determined at the widest egg diameter. The in vitro sperm-egg fusion assay was performed as described previously (28). Isolated eggs were treated with hyaluronidase in M199*+0.3% BSA to remove cumulus cells and then treated with 10 μg of chymotrypsin/ml in M199*+0.3% BSA for 3 min to loosen the ZP. The treated eggs were transferred through three clean drops of medium using a narrow-bore pipette to mechanically remove the loosened zonae. Zona-free eggs were preloaded with DAPI dihydrochloride at 10 μg/ml in M199*+0.3% BSA for 15 min at 37°C in 5% CO_2. After DAPI treatment, the eggs were washed through three drops of clean M199*+0.3% BSA. The eggs were allowed to recover for 3 h before insemination with caudal epididymal sperm incubated in M199*+3.0% BSA for 3 h. Fused sperm can be identified by the fluorescent staining with preloaded DAPI.

Time course analysis of in vitro fertilization. The time course analysis of in vitro fertilization was performed as described previously (1). Briefly, for each round of analysis, one *Zpbp2* heterozygous male and one *Zpbp2*-null male were used, and their caudal epididymal sperm were capacitated for 2 h in 0.2 ml of

TYH medium before fertilization. For each time point, four female C57/129S5 mice, 2 to 3 months old, were superovulated, and the cumulus-oocyte complexes were recovered 15 to 16 h after the administration of hCG in 0.2 ml of TYH medium. To minimize the difference in the quality of recovered oocytes, the cumulus-oocyte complexes in one oviduct were separated from those in the other oviduct, and the two separate pools were then fertilized with capacitated sperm from either the *Zpbp2* heterozygous male or the *Zpbp2*-null male. For fertilization, capacitated sperm were added to a final concentration of 1.5×10^5/ml, followed by incubation for 3 to 6 h at 37°C under 5% CO_2 in air. At the end of incubation, the eggs were briefly treated with hyaluronidase, fixed with 2% formaldehyde, and stained with DAPI. Embryos containing enlarged sperm head in the cytoplasm or two pronuclei were recorded as fertilized embryos.

Western blot analysis of proteins remaining in acrosome-reacted sperm. Mouse sperm were release from caudal epididymis in M2 medium and incubated at 37°C for 30 min. The sperm were then washed with M2 medium and divided into four aliquots. Calcium ionophore, A23187 (Sigma), was added to a final 10 μM concentration to induce acrosome reaction, and the four aliquots were incubated at 37°C for 0, 10, 30, and 60 min, respectively. The treated sperm were centrifuged to remove soluble proteins with the medium, and the sperm pellets were extracted with radioimmunoprecipitation assay (RIPA) buffer (50 mM Tris-HCl [pH 7.4], 1% NP-40, 0.5% sodium deoxycholate, 0.1% sodium dodecyl sulfate, 150 mM sodium chloride) to monitor proteins remained on acrosome-reacted sperm by Western blot analysis.

Serial extraction of acrosomal proteins. Two different serial extraction methods of mouse sperm proteins were used, and protease inhibitor (Roche) was used in all extraction buffers. The three-step (sonication, high-salt, and RIPA) extraction method was performed as described previously (51) with minor modifications. Briefly, mouse sperm were release from caudal epididymis in M2 medium and washed with PBS. Sperm were subjected to sonication with Branson Sonifier 250 six times at 20% duty cycle and output level 4. After centrifugation at 20,000 × *g* at 4°C for 10 min, the sonicated supernatant (SS fraction) was separated from the sperm pellets. Sperm pellets were extracted in the high-salt buffer (1 M KCl, 20 mM Tris-HCl [pH 7.4]) at 4°C overnight. After centrifugation, the supernatant contained high-salt extracted proteins (HS fraction), and the cell pellets were further extracted with RIPA buffer. Similarly, the two-step, M-PER/RIPA, extraction used M-PER buffer (Pierce) to permeabilize sperm membrane and extract soluble sperm proteins at room temperature for 5 min. After centrifugation, the M-PER supernatant (M-PER fraction) was separated, and the cell pellets were further extracted with RIPA buffer. Equal aliquots of extracted proteins from each step were used to compare the relative abundance in each fraction. For Western blot analysis, the goat anti-ZPBP1 polyclonal antibody (G176) was used at a dilution of 1:1,000, and the rabbit anti-ZPBP2 peptide antibody was used at a dilution of 1:15,000. The anti-green fluorescent protein (anti-GFP) antibody (Sigma G6539) was used at a dilution of 1:3,000.

Statistical analysis methods. Statistical significance was determined by using the two-tailed unpaired Student *t* test assuming unequal variances.

RESULTS

Identification of the *ZPBP* gene family by in silico subtraction. To expand our understanding of the unique physiology of germ cells and uncover candidate genes as novel contraceptive targets, we took advantage of publicly available expressed sequence tag (EST) and microarray data to identify conserved genes preferentially expressed in germ cells in silico (24, 38). One of the identified novel EST clusters matched an adult mouse testis cDNA (GenBank accession no. AK006058) annotated as a homolog of the testis-specific ZP binding protein 1 (*Zpbp1*) gene, suggesting possible roles of this protein in gamete interactions. To verify the presence of this transcript in the testis, 5′RACE analysis and RT-PCR cloning were performed, and the verified sequence was submitted to GenBank (AY251601). Based on its homology with mouse *Zpbp1*, this paralogous gene was named *Zpbp2*. *Zpbp1* was originally identified in pigs (D17572 [31]), and the orthologs of *Zpbp1* from mouse (D17569) and human (D17570) were also identified. By mapping to the reference genome sequence, mouse *Zpbp1* and *Zpbp2* demonstrated similar eight-exon configurations and are located on chromosome 11; the mouse *Zpbp1* gene is much bigger, spanning 184 kb, compared to the mouse *Zpbp2* gene, which only spans 7.5 kb. Using mouse *Zpbp2* sequences to search EST databases, we also identified and cloned the rat *Zpbp2* (AY251605) and human *ZPBP2* (AY251603) orthologs.

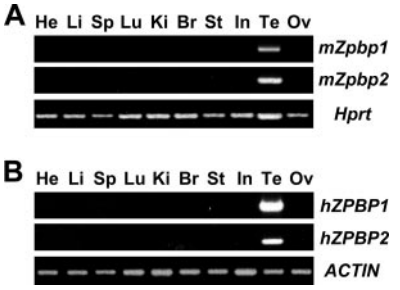

FIG. 1. *ZPBP* genes are testis-specific in mice (m) and humans (h). The testis-specific expression of *mZpbp1* and *mZpbp2* (A) and *hZPBP1* and *hZPBP2* (B) are shown by multitissue RT-PCR. *Hprt* and β-*ACTIN* were used as loading controls. He, heart; Li, liver; Sp, spleen; Lu, lung; Ki, kidney; Br, brain; St-stomach; In-intestine; Te, testis; Ov, ovary.

To examine the efficacy of our in silico subtraction process, we confirmed the testis-specific expression of *Zpbp1* (31) and *Zpbp2* in both mice and humans by multitissue RT-PCR (Fig. 1A and 1B) and Northern blot analysis (data not shown). After extensive BLAST searches using the mouse *Zpbp1* and *Zpbp2* sequences, no other paralogs besides *Zpbp1* and *Zpbp2* were identified in mice, rats, and humans. Thus, we grouped these two genes into a *ZPBP* gene family.

ZPBP1 and ZPBP2 are acrosomal proteins found specifically in male germ cells. To examine the cell types expressing the *ZPBP* genes and their temporal expression patterns during mammalian spermatogenesis, we performed in situ hybridization and found that both mouse *Zpbp1* and *Zpbp2* are expressed exclusively in male germ cells from the mid-pachytene spermatocyte stage to the early elongating spermatid stage (see the supplemental material). Although the transcripts of both *Zpbp1* and *Zpbp2* begin to accumulate in pachytene spermatocytes with essentially identical expression patterns, their protein products are first detectable by immunostaining in the proacrosomal granule in step 2 to 3 round spermatids (data not shown). With the progression of acrosomal biogenesis, ZPBP1 and ZPBP2 begin to show different intra-acrosomal localizations. ZPBP1 is present throughout the entire acrosome during spermiogenesis, whereas ZPBP2 is concentrated in the acrosomal granule in early spermatids (Fig. 2A) and subsequently distributed along the rostral ridge of the acrosome as a sharp band (Fig. 2B).

Cross-species analysis of ZPBP family members. With the rapidly growing collections of EST and WGS (for whole genome shotgun) libraries, we were able to perform BLAST searches to find short matches of both *Zpbp1* and *Zpbp2* in the genomes of a wide variety of mammalian species, including marsupials (opossum [*Monodelphis domestica*]) and monotremes (platypus [*Ornithorhynchus anatinus*]). Outside of the mammalian lineage, we also obtained short partial ZPBP matches in the genomes of chicken (*Gallus gallus*) and Western clawed frog (*Xenopus tropicalis*), and the most conserved regions were used to design degenerate primers for cloning. We cloned both *ZPBP1*

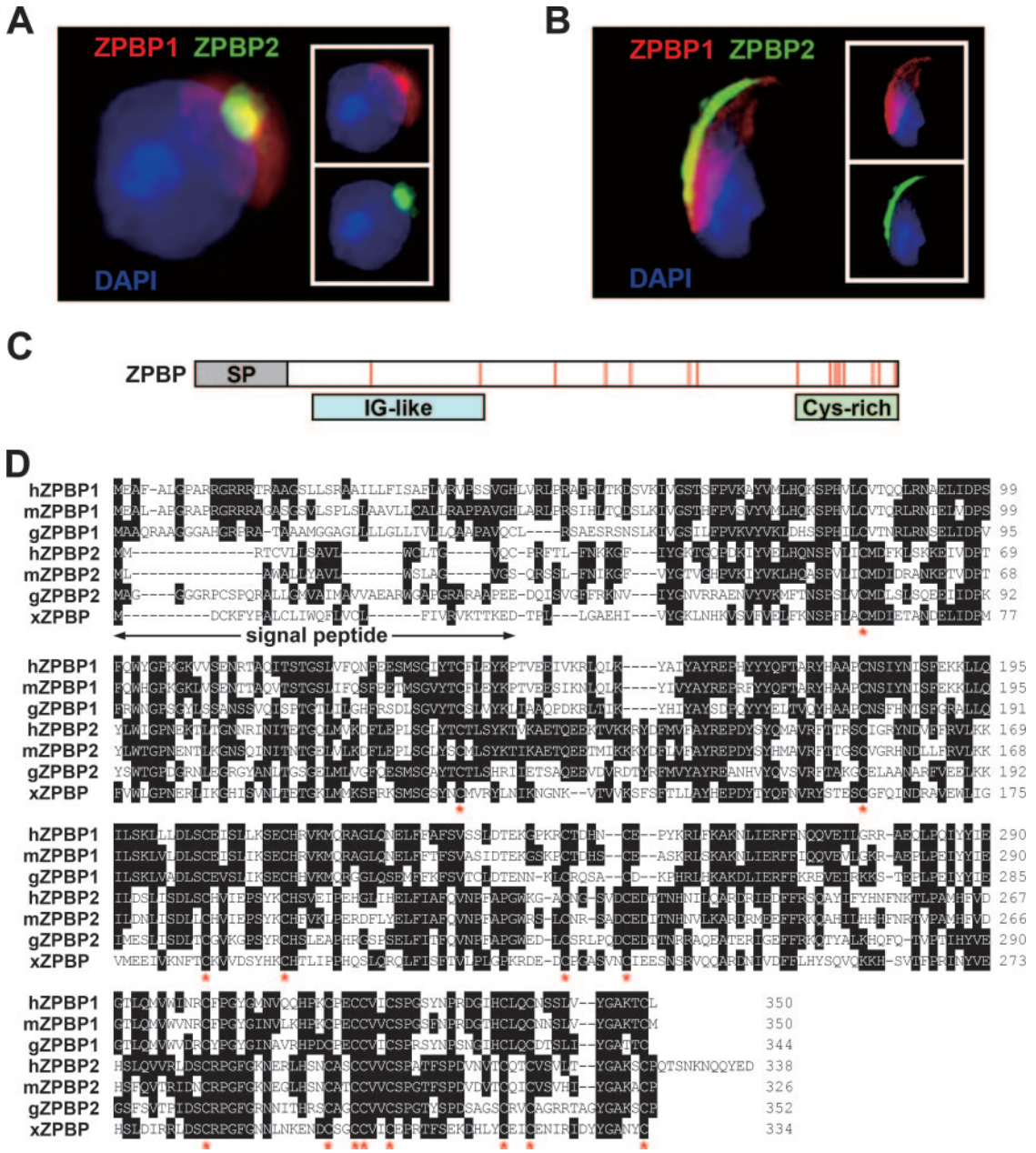

FIG. 2. ZPBP proteins are intra-acrosomal proteins and present in amphibian, avian, and mammalian species. (A and B) Immunofluorescence microscopy showed different intra-acrosomal localizations of mouse ZPBP1 (red) and ZPBP2 proteins (green) in step 5 round spermatids (A) and in mature spermatozoa (B). (C) Domain structures of ZPBP proteins. The signal peptide was predicted by using the SignalP server (http://www.cbs.dtu.dk/services/SignalP) (14), and the immunoglobulin-like (IG-like) domain was predicted by using the SMART database (http://smart.embl-heidelberg.de) (23). Red bars represent the 15 conserved cysteines (Cys) among ZPBP proteins, and 8 of these Cys are located near the C terminus. (D) Protein sequence alignment shows the 15 conserved cysteines (red asterisks) outside of the signal peptide region as the defining feature of the ZPBP protein family. h, human; m, mouse; g, chicken (*G. gallus*); x, frog (*X. laevis*).

(AY563140) and *ZPBP2* (AY575015) from chicken testis cDNA. Since the frog species preferred for fertilization studies is *Xenopus laevis*, we also cloned the frog *ZPBP* (EF363028) from *Xenopus laevis* testis cDNA. Protein sequence analysis revealed that both ZPBP1 and ZPBP2 proteins have an N-terminal signal peptide, an immunoglobulin-like domain, a C-terminal Cys-rich region, and several predicted N-glycosylation sites (Fig. 2C). When aligned, it is apparent that all 15 cysteines outside of the predicted signal peptide region are conserved among ZPBP proteins (Fig. 2D), and the predicted secondary structures (data not shown) suggest that all ZPBP family members share a similar conformation dependent on conserved disulfide bonds.

Alignment analysis (Fig. 2D) shows that frog *ZPBP* is the ortholog of mouse *Zpbp2*. After careful examination of the conserved neighboring genes, *Grb10-Znfn1a1-Zpbp1* and *Grb7-Znfn1a3-Zpbp2*, located at the syntenic loci in mamma-

lian genomes (19), we were unable to identify a *ZPBP1* ortholog at the syntenic locus in the *Xenopus tropicalis* genome assembly version 4.1. RT-PCRs using two different degenerate primer pairs designed from sequences conserved among *ZPBP1* members also failed to amplify a *ZPBP1* ortholog from frog testis cDNA. We conclude that *Xenopus* species possess only one *ZPBP* gene. Outside of amphibians, extensive BLAST searches for the *ZPBP* family members using genome databases, whole-genome shotgun sequence databases, and EST databases failed to identify any *ZPBP* gene members in teleost fish (bony fish) species, indicating major differences between teleost fishes versus birds, amphibians, and mammals in the process of spermatogenesis and/or fertilization (see Discussion).

Generation of *Zpbp1* and *Zpbp2* knockout mice. To study the physiological roles of ZPBP1 and ZPBP2 proteins, we generated targeted deletions of the signal peptide encoding regions of the mouse *Zpbp1* and *Zpbp2* genes by homologous recombination in mouse ES cells (Fig. 3A to D), resulting in $Zpbp1^{tm1Zuk}$ and $Zpbp2^{tm1Zuk}$ targeted alleles, respectively (herein called $Zpbp1^{-}$ and $Zpbp2^{-}$). Chimeric males generated from targeted ES cells were bred to C57BL/6J (B6) females to generate F_1 heterozygous mice, and heterozygous littermates were intercrossed to produce homozygous mutant mice. There was no distortion of the Mendelian ratio in offspring generated from heterozygous mating pairs, and both *Zpbp1* homozygous null ($Zpbp1^{-/-}$) and *Zpbp2* homozygous null ($Zpbp2^{-/-}$) mice showed no apparent defects in development or ability to thrive (consistent with their testis-specific expression). The testicular weights of $Zpbp1^{-/-}$ males (86.9 ± 3.1 g; $n = 8$) and $Zpbp2^{-/-}$ males (88.7 ± 2.6g; $n = 10$) were similar to that of their wild-type (88.2 ± 2.7 g; $n = 6$) and heterozygous siblings (89.3 ± 2.2 g; $n = 10$). Northern blot (Fig. 3E) and Western blot (Fig. 3F) analyses demonstrated the absence of mRNA and proteins, respectively, in the testes of homozygous *Zpbp1* and *Zpbp2* mutant mice and confirmed that both targeted mutant alleles are null alleles. The inability to detect ZPBP2 protein in sperm from $Zpbp1^{-/-}$ mice (Fig. 3F) was ascribed to severely disrupted acrosome biogenesis in *Zpbp1*-null spermatids (see below).

***Zpbp2*-null males show reduced fertility and produce sperm with subtle deformation.** When $Zpbp2^{+/-}$ males were housed with either $Zpbp2^{+/-}$ or $Zpbp2^{-/-}$ females for a 6-month period, normal fecundities were observed (Fig. 3G and H). In contrast, $Zpbp2^{-/-}$ male mice showed significantly decreased fecundity compared to heterozygous males (Fig. 3G and H).

Although sperm counts and sperm motility were similar between $Zpbp2^{+/-}$ and $Zpbp2^{-/-}$ males (data not shown), almost all of the *Zpbp2*-null sperm showed subtle deformation, including a shortened apical hook, smaller apical angle, and bulges in close approximation of the acrosome region (Fig. 4B to E). The absence of bulges on acrosome-reacted sperm indicated that the bulges are acrosomal (Fig. 4D), and electron microscopy demonstrated that the bulges are formed from pockets of excessive acrosome folding onto itself (Fig. 4G and H). These affected structures matched the localization of ZPBP2 (Fig. 2B), suggesting structural roles of ZPBP2 in the compaction of the acrosome along the acrosome ridge.

To determine the cause of the decreased fecundity in the $Zpbp2^{-/-}$ males, we performed various sperm-oocyte binding and fertilization assays in vitro (Fig. 4I to L). Whereas *Zpbp2*-null sperm showed normal binding to the ZP (Fig. 4J) and normal fusion with zona-free eggs (Fig. 4L), in vitro fertilization rates with zona-intact eggs were slower (Fig. 4K), resulting in fewer oocytes fertilized (Fig. 4I). This indicates that the delayed fertilization most likely involves reduced zona penetration in the absence of ZPBP2.

***Zpbp1* knockout males are infertile secondary to globozoospermia.** To study the function of ZPBP1 and possible redundancy of the ZPBP proteins, we produced *Zpbp1* mutant and *Zpbp1*/*Zpbp2* double mutant mice. Like $Zpbp2^{-/-}$ females, $Zpbp1^{-/-}$ females and $Zpbp1^{-/-}$/$Zpbp2^{-/-}$ females showed normal fertility (Fig. 3I and J). For both *Zpbp1* heterozygous ($Zpbp1^{+/-}$) and double heterozygous ($Zpbp1^{+/-}$/$Zpbp2^{+/-}$) males, although higher percentages (>20%) of sperm with abnormal morphology were observed, their fecundity was still comparable to wild-type males (Fig. 3I and J). However, the proportions of abnormal sperm in $Zpbp1^{+/-}$/$Zpbp2^{-/-}$ males were higher, and the fecundity and fertility dropped to 3.4 ± 0.40 pups/litter and 3.8 ± 0.60 litters in 6 months (Fig. 3I and J). These observations suggest dosage effects of the paralogous *Zpbp1* and *Zpbp2* genes in sperm morphogenesis.

In contrast to the decreased fecundity observed in $Zpbp2^{-/-}$ males, homozygous *Zpbp1*-null ($Zpbp1^{-/-}$) males and *Zpbp1*/*Zpbp2* double-null ($Zpbp1^{-/-}$/$Zpbp2^{-/-}$) males were all sterile (Fig. 3I and J). The sperm counts were similar between wild-type males ($11.8 \times 10^6 \pm 0.9 \times 10^6$; $n = 7$) and *Zpbp1*-null ($12.8 \times 10^6 \pm 1.0 \times 10^6$; $n = 7$) or *Zpbp1*/*Zpbp2* double-null ($11.3 \times 10^6 \pm 1.2 \times 10^6$; $n = 5$) males. However, infertility was associated with severe deformation of the spermatozoa (Fig. 5B and C; 100% abnormal morphology), with the majority of caudal epididymal sperm demonstrating round-headed morphology with a coiled tail around the sperm nucleus. In addition, *Zpbp1*-null sperm showed dramatically and statistically reduced sperm motility (10.0% ± 3.8% motile; $n = 6$) with no forward motility compared to controls (68.0% ± 5.2% motile; $n = 6$). Further examination using *Zpbp1*-null sperm carrying the *Acr-EGFP* transgene (34) or immunofluorescence labeling with anti-ZPBP2 antibody showed that the acrosome was absent in >80% of the *Zpbp1*-null sperm. The remaining <20% of sperm had only abnormally shaped acrosomal remnants (data not shown). The proportions of *Zpbp1*-null spermatozoa showing coiled flagellum increased from proximal caput epididymis (9.3% ± 1.7%, $n = 4$) to caudal epididymis (79.5 ± 2.8, $n = 4$), suggesting that the transformation of noncoiled proximal caput epididymal sperm (Fig. 5D) to coiled caudal epididymal sperm (Fig. 5E) occurs during epididymal maturation, similar to *Gopc* knockout mice (18, 43, 50; see also Discussion).

Using electron microscopy, additional ultrastructural abnormalities were observed in all spermatozoa, including misshapen nuclei, detached flagella, and disorganized mitochondria trapped inside excessive cytoplasmic droplets (Fig. 5F and G). As early as step 6 to 8 spermatids, minor acrosomal abnormalities, including a dilated acrosome (Fig. 5I), detached or eccentric acrosomal granules, and occasional nuclear indentation by the dilated acrosome were observed in spermatids and spermatozoa in $Zpbp1^{-/-}$ testis. During spermiogenesis in the mouse, the compaction of the acrosome begins around step 6 and results in a completely flattened vesicle with an electron-

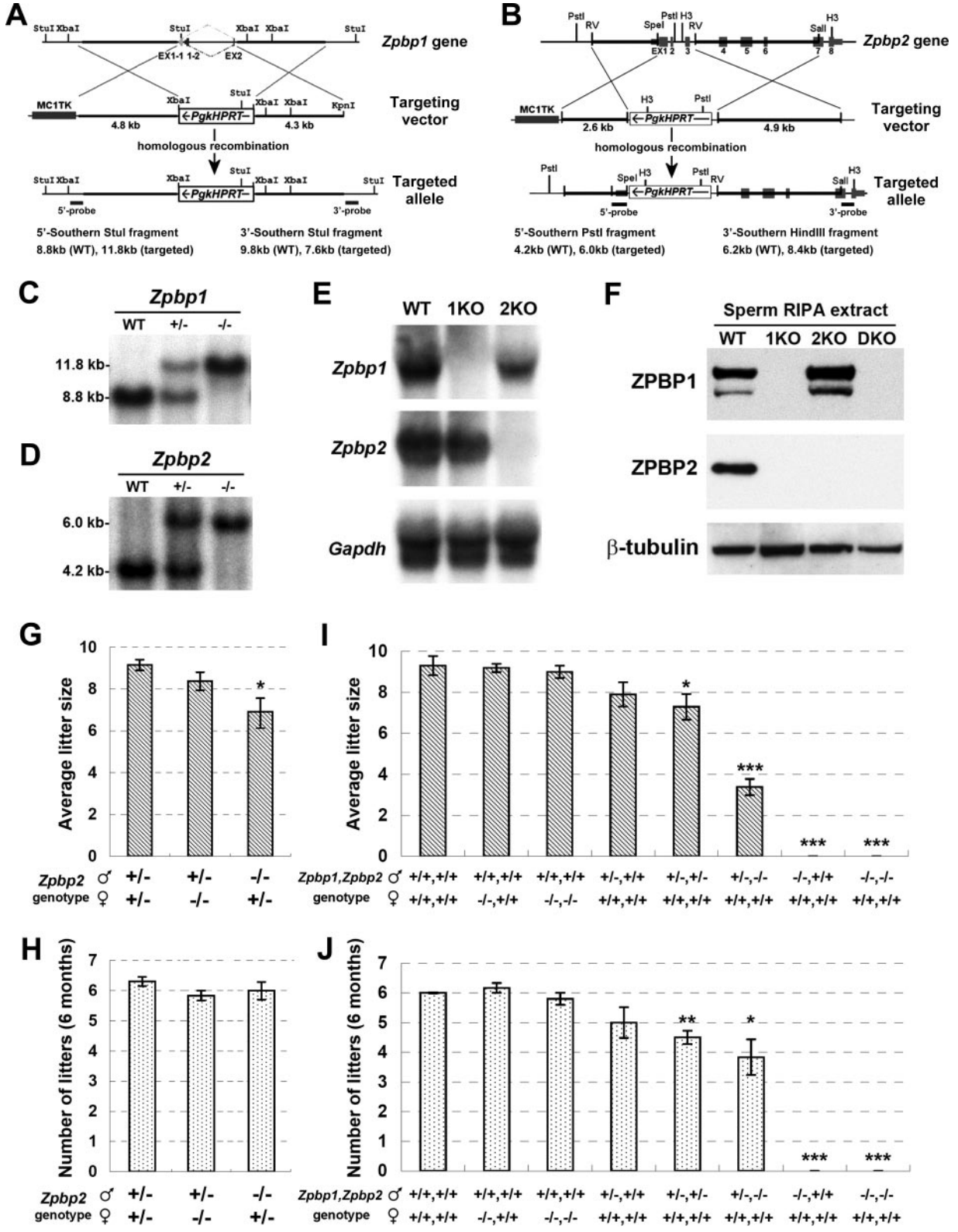

FIG. 3. Targeted disruption of *Zpbp1* and *Zpbp2* results in a deficiency of both transcripts and proteins and male fertility defects. (A and B) Gene targeting strategies for *Zpbp1* (A) and *Zpbp2* genes (B). (C and D) Southern blot results for wild-type and mutant alleles of *Zpbp1* (C) and *Zpbp2* (D) with 5′ probes. (E) Northern blot analysis of total testis RNA confirmed the absence of gene-specific transcripts in null (KO) testes. (F) Western blot analysis also confirmed the absence of ZPBP proteins in null sperm. (G to J) Six-month fertility data for mice of different genotypes. *, $P < 0.05$; **, $P < 0.005$; ***, $P < 0.0005$.

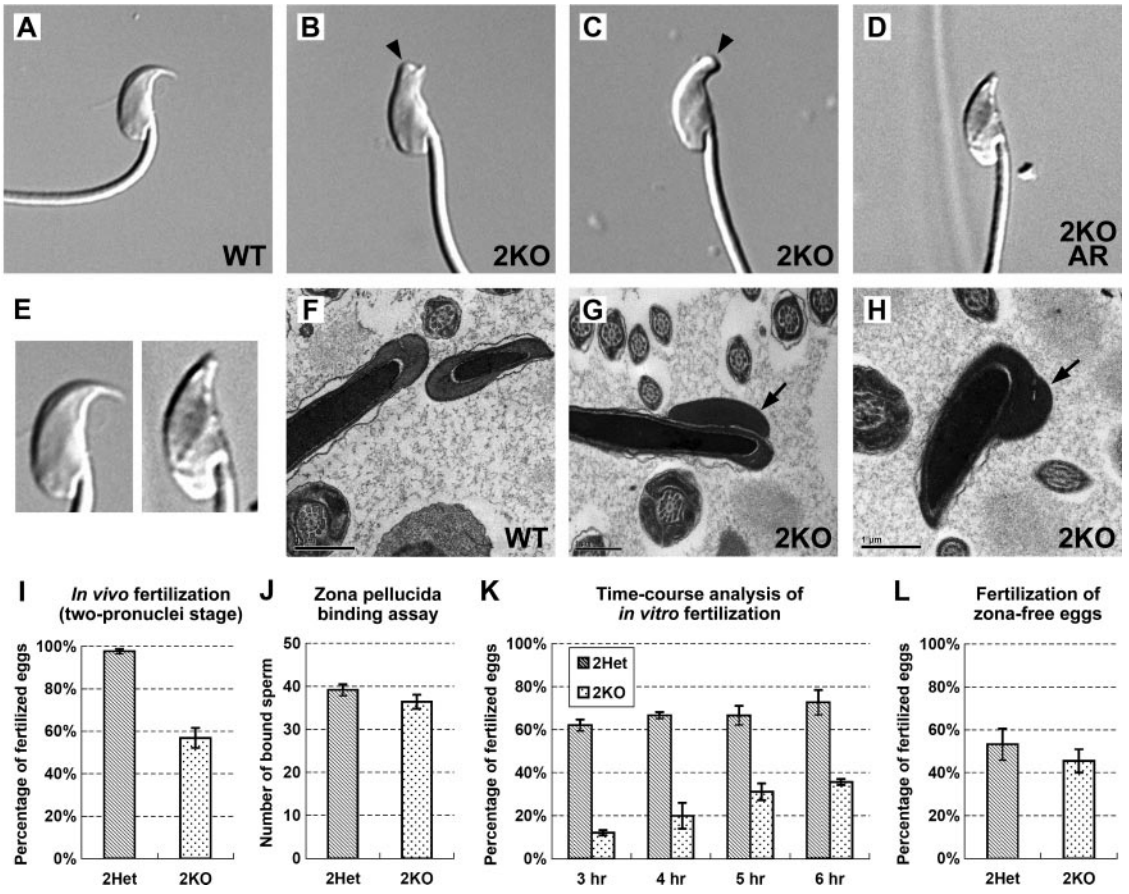

FIG. 4. *Zpbp2*-null spermatozoa show subtle deformations and impaired fertilization. (A to E) Light microscopy analysis of wild-type (WT) (A) and *Zpbp2*-null sperm (2KO) (B to D). *Zpbp2*-null sperm showed bulges along the dorsal ridge (arrowheads in panels B and C) over the acrosome. (D) The bulges were removed from *Zpbp2*-null sperm after A23187-induced acrosome reaction (2KO-AR). (E) *Zpbp2*-null sperm (D, right) also showed a shortened apical hook and smaller apical angle compared to wild-type sperm (A, left). (F to H) Electron microscopic analysis of wild-type (F) and *Zpbp2*-null (G and H) sperm. The acrosomal bulges on *Zpbp2*-null sperm are indicated by arrows. (I to L) In vitro binding and fertilization assays for *Zpbp2* heterozygous (2Het) and homozygous (2KO) males. The numbers of animals or eggs used for each assay are as follows: I, $n = 8$; J, 48 eggs; K, $n = 3$, 1,303 eggs; L, $n = 3$, 277 eggs.

dense acrosomal matrix in step 9 wild-type spermatids (Fig. 5J) when the acrosome forms tight association with the Sertoli cell and anchors the nucleus to the junctional structures (40). In contrast, step 9 *Zpbp1*-null spermatids (Fig. 5K) show a dilated acrosome, indicating failure in the compaction of the developing acrosome. Acroplaxome (20), an actin-keratin-containing structure anchoring the developing acrosome to the nuclear membrane, was found to be present as an electron-dense layer (Fig. 5I and K), suggesting that the acrosome-acroplaxome interactions are intact in *Zpbp1*-null spermatids.

In elongating spermatids, the acrosome is seen as a compact organelle anchoring the nucleus to the Sertoli cell at Sertoli-spermatid junctions in wild-type spermatids (Fig. 5L). In contrast, close association of the spermatid nucleus with the Sertoli cell is disrupted, and abnormal vesicles can be found within the Sertoli cell cytoplasm of *Zpbp1*$^{-/-}$ testes (Fig. 5M). The filamentous actin (F-actin) bundles surrounding these vesicles suggest that these vesicles are internalized from the Sertoli-spermatid junctions adjacent to the acrosome region of spermatids. Other images with the dilated acrosome undergoing fragmentation further confirm that these internalized vesicles were acrosome fragments coated with junctional structures (Fig. 5N and O). Although small amounts of excessive acrosomal contents may be removed normally through tubulobulbar complexes (44), the profound fragmentation and degradation of dilated acrosomes observed in *Zpbp1*-null spermatids is not seen in wild-type spermatids or described in other knockout mouse models. When analyses were performed with double-null males (data not shown), the fragmentation and degradation of acrosomes were identical to *Zpbp1* single-null males. This is consistent with our observation that consequences of ZPBP1 deficiency are so severe as to compromise accumulation of ZPBP2 protein and mask any separable roles of ZPBP2.

Different release kinetics and posttranslational processing between ZPBP1 and ZPBP2. ZPBP1 has been reported to persist in acrosome-reacted sperm (31, 51), and ZPBP1 is released by the A23187-induced acrosome reaction (42). To understand why more significant phenotypes are observed in spermatids and spermatozoa lacking ZPBP1 in addition to the more widespread intra-acrosomal localization of ZPBP1 compared to ZPBP2 (Fig. 2A and B), we compared the release kinetics of ZPBP1 and ZPBP2 from acrosome-reacted sperm

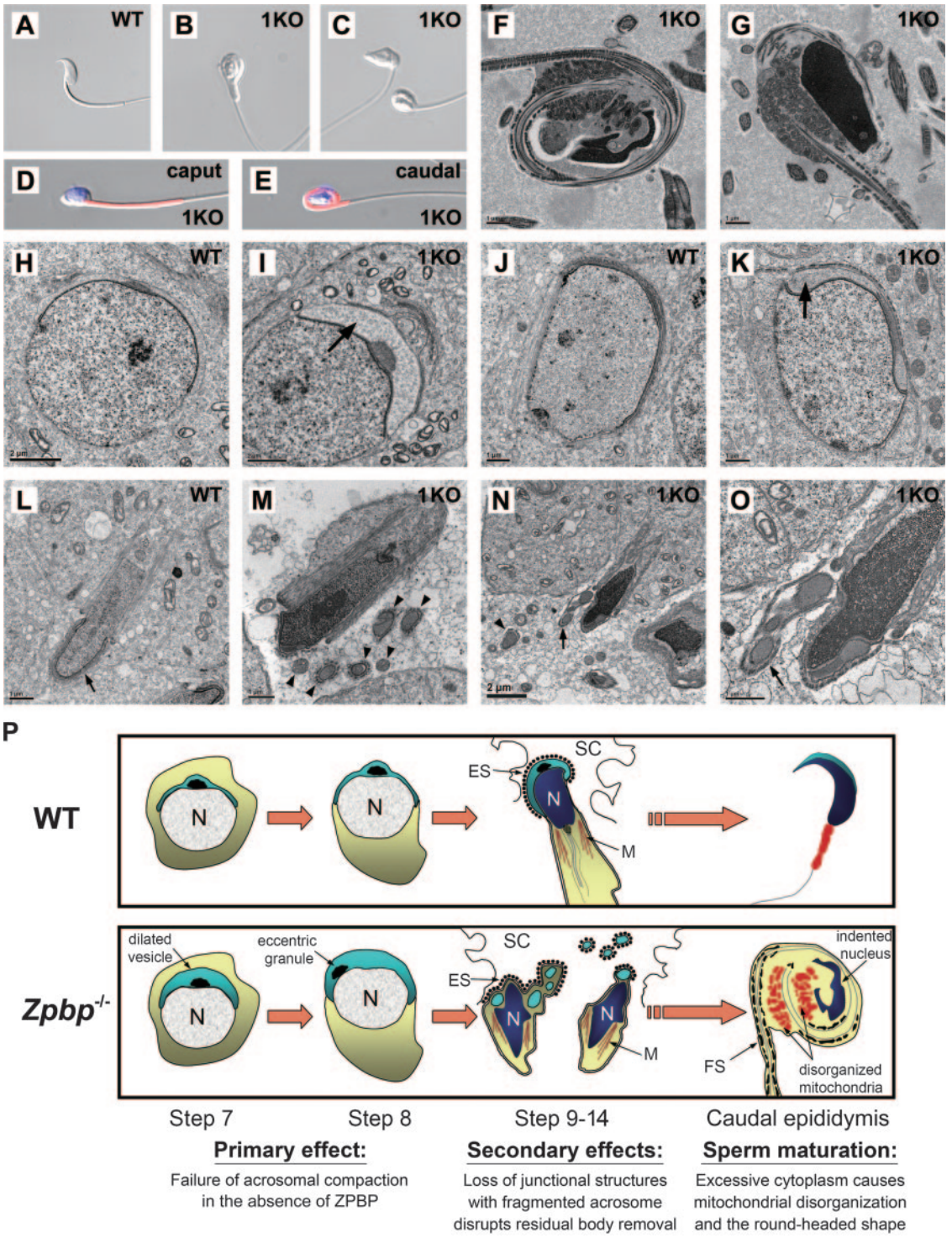

FIG. 5. *Zpbp1*-null spermatozoa exhibit morphological defects with a round-headed appearance and the absence of an acrosome. (A to C) *Zpbp1*-null (1KO) sperm exhibit a disorganized midpiece coiled around an abnormally shaped sperm nucleus (B and C) in contrast to wild-type (WT) sperm (A). (D and E) The coiling of the midpiece occurs mostly during epididymal maturation. In the proximal caput epididymis, most sperm have a straight midpiece and variable amounts of excessive cytoplasm (D). In contrast, after undergoing epididymal maturation, most sperm in the caudal epididymis have a coiled midpiece. Red, MitoTracker; blue, DAPI. (F and G) Electron microscopic images of caudal epididymal *Zpbp1*-null sperm revealed retained cytoplasmic droplets and disorganized mitochondria encircling the abnormally shaped nuclei. (H to K) Electron microscopic images of step 6 to 9 spermatids. In step 7 (I) and early step 9 (K) *Zpbp1*-null spermatids, acrosomes (arrows) fail to undergo compaction as wild-type spermatids at comparable stages (H and J). (L to O) Electron microscopic images of step 9 to 14 spermatids demonstrate compact acrosome (arrow) in wild-type (WT) spermatids (L). In contrast, fragmented acrosomes (arrowheads in panels M and N) and an acrosome undergoing fragmentation (arrow in panel N and the enlarged view [panel O]) from *Zpbp1*-null (1KO) spermatids were observed in Sertoli cells as vesicles surrounded by F-actin bundles from apical ectoplasmic specializations. (P) Schematic representation of the electron microscopy results showing the progressive changes leading to the round-headed sperm in *Zpbp1*$^{-/-}$ males. N, nucleus; SC, Sertoli cells; ES, apical ectoplasmic specializations; M, manchette; FS, fibrous sheath.

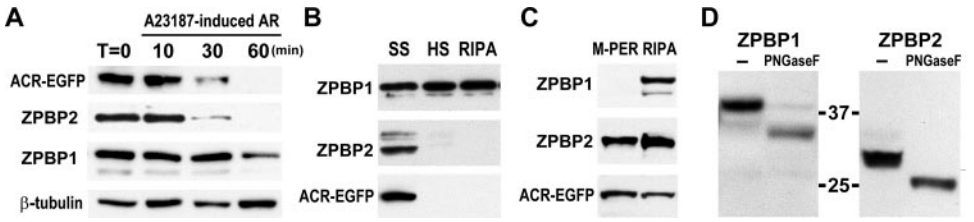

FIG. 6. Mouse ZPBP1 and ZPBP2 display different release kinetics and protein processing. (A) Time course Western blot analyses of Acr-EGFP, ZPBP1, ZPBP2, and β-tubulin remaining in *Acr-EGFP* mouse sperm after the A23187-induced acrosome reaction (AR). β-Tubulin was used as loading control. (B and C) Western blot analysis of ZPBP1, ZPBP2, and Acr-EGFP from different fractions after the three-step (B) or the two-step (C) serial extraction of *Acr-EGFP* sperm. SS, sonicated supernatant; HS, high-salt extraction; RIPA, RIPA extraction; M-PER, M-PER permeabilization. (D) Western blot analysis of sperm proteins treated without (−) and with PNGase F. Anti-ZPBP1 and anti-ZPBP2 antibodies were used as shown.

using *Acr-EGFP* (for prepropeptide proacrosin-enhanced GFP fusion transgene) mice (34), in which soluble ACR-EGFP accumulates in the acrosome. A time course Western blot analysis of proteins remaining in acrosome-reacted sperm showed that the soluble ACR-EGFP and ZPBP2 were mostly released by 30 min after the acrosome reaction, whereas ZPBP1 remained detectable in the sperm 60 min after the acrosome reaction (Fig. 6A), suggesting tighter association with the acrosomal matrix. By using a modified two-step sonication/high-salt extraction procedure (51), we observed persistent association of ZPBP1 protein with the acrosomal matrix in all three sequential extraction steps, while soluble ACR-EGFP and ZPBP2 are readily released after sonication-mediated disruption of the outer acrosomal membrane (Fig. 6B). When we replaced sonication with a mild membrane permeabilization reagent, M-PER, preferential extraction of ZPBP2 and ACR-EGFP was observed, with negligible levels of ZPBP1 extracted (Fig. 6C). Taken together, these results indicate that ZPBP2 is readily soluble after either the acrosome reaction or the permeabilization of the acrosomal membrane, while the slower release of ZPBP1 supports a close association of ZPBP1 with the acrosomal matrix through noncovalent interactions.

Because of the presence of putative N-glycosylation sites in both ZPBP1 and ZPBP2 proteins, we also performed Western blot analysis with the deglycosylated mouse sperm proteins. Removal of the N-linked oligosaccharides with peptide N-glycosidase F (PNGase F) revealed that the 38-kDa ZPBP1 band collapsed down to 34 kDa and the 29-kDa ZPBP2 band collapsed down to 25 kDa (Fig. 6D). Although 34 kDa is the expected size for the mature peptide portion of ZPBP1, the observed 25-kDa band for deglycosylated ZPBP2 is much smaller than the expected 35-kDa mature peptide. That the anti-peptide ZPBP2 antibody was generated against amino acids 62 to 76 within the 326-amino-acid open reading frame of ZPBP2 and amino acids 62 to 326 alone account for an apparent molecular mass of 30.4 kDa suggests additional proteolytic processing in the C-terminal region of ZPBP2. These results reveal different biochemical properties, including release kinetics and posttranslational processing, between ZPBP1 and ZPBP2 in mouse sperm.

DISCUSSION

We demonstrated an unexpected aspect of the intra-acrosomal ZPBP proteins as integral structural components for the compaction of the acrosomal matrix and the normal fertility of knockout females confirms the specific functions of ZPBP1 and ZPBP2 in the male germ cells. The earliest phenotype in mouse spermatids lacking ZPBP1 is failure of acrosome compaction, leading to a dilated acrosome overlying the sperm nucleus. During the elongation phase of spermiogenesis, the dilated acrosome undergoes fragmentation, and the Sertoli-spermatid junctions are internalized by Sertoli cells with the acrosome fragments (Fig. 5P). In contrast, loss of ZPBP2 results in decreased fecundity and subtle sperm head deformities that correspond to the discrete localization of ZPBP2 along the rostral ridge of spermatozoa. Since several muroid rodents (in superfamily *Muroidea*) with a variety of less prominent apical hook and nonhooked sperm heads exist in nature (6, 7), the morphological changes of *Zpbp2*-null sperm are unlikely to be prohibitive to their fertilization potentials, thus suggesting that the reduced zona penetration is responsible for the decreased fecundity. In double-knockout mice, the effects of disrupted ZPBP1 preclude any appreciation of independent ZPBP2 function. This may reflect the wider distribution of ZPBP1 in the entire acrosome (Fig. 2A and B) and the closer integration of ZPBP1 within the acrosomal matrix as shown in the slower release kinetics after the acrosome reaction (Fig. 6A). In addition, the delayed zona penetration by *Zpbp2*-null sperm suggests that ZPBP proteins are important acrosomal matrix components involved in interacting with the ZP during sperm penetration.

Insights from the cross-species analysis of the *ZPBP* gene family. The in silico identification and experimental validation of *ZPBP2*, the paralog of the previously reported *ZPBP1* (30, 31, 51), completes the mammalian *ZPBP* gene family. By comparative cross-species studies, we further established the coexistence of both *ZPBP* members in birds and mammals, and the presence of a single *ZPBP2* ortholog in *Xenopus*. Based on the absence of a *ZPBP1* ortholog among conserved adjacent genes duplicated at syntenic loci in the *Xenopus tropicalis* draft genome, we conclude the absence of a *ZPBP1* ortholog is the result of gene loss after a regional duplication event and suggest that frog ZPBP (32% amino acid identity with mouse and human ZPBP2) likely demonstrate activities of both mammalian ZPBP1 and ZPBP2. These observations, combined with the ease of performing biochemical experiments using *Xenopus* eggs, suggest that *Xenopus* may be an alternative model organism system for future analysis of ZPBP functions during sperm penetration.

Since ZP2 is reported to be the in vitro binding partner of ZPBP1 (30), we also examined the evolution of ZP2 among the well-conserved ZP protein family members found in the egg investment. Among the three groups of ZP proteins, ZP3 and ZP1/ZP4 groups are highly conserved components of the egg investment from teleost fishes to mammals (29, 41). Interestingly, *ZP2* orthologs are only found in frogs, birds, and mammals (but not in teleosts [bony fishes] and more primitive vertebrate species) (41), matching the distribution pattern of *ZPBP* gene family members that we report here. Although a possible coevolutionary relationship among ZP2 and ZPBP proteins requires further analyses, it is noteworthy that this pattern also correlates with another transition in the fertilization process in evolution. In teleosts, the micropyle on the egg investment provides an opening that allows the acrosomeless sperm to swim through to achieve sperm-egg fusion (10). In contrast, all living tetrapod vertebrates (amphibians, reptiles, birds, and mammals) have eggs that lack a micropyle and are completely encircled by an egg investment, thus necessitating the sperm acrosome reaction for penetration (2, 25). This raises an interesting question about a coevolutionary relationship developed between the interacting proteins (ZP2 from eggs and ZPBPs from sperm) and the mode of fertilization (penetration of completely encircled egg investment in the absence of micropyle) during the evolution of terrestrial tetrapod species from the ancestral fish species. Future comparative studies among different fish species may shed more light on this question.

Potential roles of ZPBP proteins during sperm penetration of the ZP. Wassarman and coworkers (3, 4) have proposed a secondary sperm binding activity of ZP2 to acrosome-reacted sperm. In contrast to the primary sperm binding activity of ZP3 that anchors sperm to the ZP surface and initiates the acrosome reaction, secondary sperm binding may be a more dynamic process during sperm penetration to allow the acrosome-reacted sperm to slice through the ZP without being immobilized by tight binding. Recently, Yu et al. (51) identified ZPBP1 as a component of the persistent acrosomal matrix overlaying the inner acrosomal membrane and suggested direct involvement of such persistent acrosomal matrix proteins in sperm penetration by antibody inhibition in their in vitro fertilization assay. The correlation between the reduced fecundity of *Zpbp2*-null males and the delayed zona penetration of *Zpbp2*-null sperm implicates ZPBP proteins in sperm-ZP interactions. Because ZPBP2 is a readily soluble acrosomal protein localized along the rostral ridge of the acrosome and the ridge is the exposed edge of acrosome-reacted sperm during zona penetration, the absence of ZPBP2 along the rostral ridge leaves only the more diffusely localized ZPBP1 to work, thus resulting in delayed zona penetration. Although we intended to study the in vivo ZP-interactions and possible redundant functions of both ZPBP proteins using knockout mice, the critical importance of ZPBP1 during spermiogenesis precluded this assessment. One possible approach to address the roles of ZPBP1 in sperm-egg binding would be to identify and separate the structural domain of ZPBP1 responsible for its assembly into the acrosome matrix from its ZP2-interacting domain. By introducing transgenes that restore the structural domains of ZPBP1 in *Zpbp1*/*Zpbp2* double-null mice, we may restore acrosome biogenesis and spermiogenesis, allowing for proper analysis of the physiological roles of ZPBP proteins during sperm-egg interactions.

Disrupted acrosome biogenesis in *Zpbp1*-null spermatids is linked to the subsequent disruption of Sertoli-spermatid junctional structures. The morphological phenotypes of *Zpbp1*-null sperm are similar to those observed in *Gopc* (for Golgi-associated PDZ- and coiled-coil motif-containing protein) knockout mice (18, 50), and the coiling of flagellum in *Zpbp1*-null and *Gopc*-null (43) sperm also occurs during epididymal maturation. Although acrosome biogenesis is disrupted at different stages and through different mechanisms in $Gopc^{-/-}$ and $Zpbp1^{-/-}$ mice, the resulting morphological defects in sperm are similar. Both knockouts have morphologically abnormal sperm with severely disrupted acrosome, abnormal nuclear shape, excessive cytoplasm, and coiled sperm tails formed during epididymal maturation.

The defective fusion of proacrosomal vesicles results in the formation of miniscule pseudoacrosomes in early *Gopc*-null round spermatids (18, 50), and apical ectoplasmic specializations are poorly formed in $Gopc^{-/-}$ testis (18). In *Zpbp1*-null spermatids, which demonstrate defective matrix protein assembly during acrosome compaction, the fragile dilated acrosome fails to withstand the exogenous morphogenic clutch force exerted through the apical ectoplasmic specializations (21). This leads to fragmentation and Sertoli cell internalization of the abnormal acrosomes, the Sertoli-spermatid junctional structures, and the apical ectoplasmic specializations. The premature loss of junctional structures (Fig. 5M to O) in turn reduces the exogenous morphogenic clutching force and contributes to the abnormal nuclear morphogenesis (Fig. 5P). Despite differences in the timing and the mechanism of defective acrosome biogenesis in $Zpbp1^{-/-}$ and $Gopc^{-/-}$ mice, the phenotypes share an inability for proper formation and maintenance of Sertoli-spermatid junctions. Interestingly, studies characterizing the important heterotypic Nectin-2–Nectin-3 interactions at Sertoli-spermatid junctions also describe abnormally shaped *Nectin-2*-null and *Nectin-3*-null sperm with disorganized mitochondria (5, 17, 35), and the reported sperm morphological phenotypes are reminiscent of the descriptions of *Zpbp1*-null and *Gopc*-null sperm, underscoring a crucial role of proper Sertoli-spermatid junctions in sperm morphogenesis.

Although multiple morphological phenotypes are observed with *Zpbp1*-null sperm, the infertility of $Zpbp1^{-/-}$ males seems largely ascribable to the severely impaired sperm motility (<10% motile sperm with no forward progression) in mature spermatozoa due to either the coiled midpiece or the disorganized mitochondrial sheath in sperm tails. Interestingly, in the proximal epididymis before the maturation process, most *Gopc*-null (43) and *Zpbp1*-null sperm carry excessive cytoplasm but not coiled tails. Because the coiling of sperm tails appears during epididymal passage for both *Gopc*-null sperm (43) and *Zpbp1*-null sperm, it is likely that reduction in the volume of excessive cytoplasm by the volume regulatory response in the hyperosmotic epididymal fluid (9) causes retraction and coiling of sperm tails into the excessive cytoplasm surrounding the sperm nucleus, supporting the detrimental effect of excessive cytoplasm on sperm maturation.

In wild-type males, most of the cytoplasm of elongated spermatids is removed as the residual body by Sertoli cells around the time of spermiation. In contrast, both *Gopc*-null (18) and

Zpbp1-null spermatids demonstrate a significant failure in the removal of excessive cytoplasm during spermiation. During the later steps of spermiogenesis, a significant amount of male germ cell cytoplasm moves to the caudal pole of spermatids and is reduced in three steps: during the elongation of spermatid, through tubulobulbar complexes, and through the removal of residual body (40, 45). All three steps require the integrity of Sertoli-spermatid junctions. It is thus likely that the impaired Sertoli-spermatid junctions in $Gopc^{-/-}$ and $Zpbp1^{-/-}$ testis directly contribute to the retention of excessive cytoplasm, which in turn disrupts sperm maturation as discussed above.

Globozoospermia is a rare human infertility disorder characterized by round-headed sperm morphology (OMIM: 102530) and absence of the acrosome (11). The *Zpbp1* and *Gopc* infertile mouse models should promote our understanding how the disruption of acrosome biogenesis affects spermiogenesis and results in round-headed sperm. Because the falciform (hook-shaped) sperm in mice differ significantly from spatulate sperm in humans, the round-headed sperm appearance cannot be the sole criteria to compare mouse and human models of globozoospermia. Careful phenotypic analyses are required to identify mouse models most closely resembling human infertilities with features including acrosomal loss, disorganization of the mitochondrial, disruption of the Sertoli-spermatid junctions, and excessive cytoplasmic droplets that impede the epididymal maturation process. Similarly, as we better understand these pathologies, discriminating between primary and secondary morphological defects in both mouse models and patients with male infertility will be increasingly important. Interestingly, one case of human globozoospermia (8) ultrastructurally showed anomalous dilated acrosomes and acrosomal remnants in Sertoli cells, suggesting that at least subsets of human globozoospermia also result from the fragmentation and degradation of abnormal acrosomes similar to the $Zpbp1^{-/-}$ phenotype.

ACKNOWLEDGMENTS

We thank Franco DeMayo and the Transgenic Core for suggestions and help with the transgenic experiments. Debra Townley and Michael Mancini in the Integrated Microscopy Core were of great help for their advice with the electron microscopy experiments. We also thank Paul Primakoff and Diana Myles for teaching gamete interaction assay techniques. The *Acr-EGFP* mice, a generous gift from Masaru Okabe, were very helpful in monitoring the acrosome status. We also thank Milan Jamrich for providing *X. laevis* tissue samples.

This research is supported by the Specialized Cooperative Centers Program in Reproduction and Infertility Research (U54 HD07495) at Baylor College of Medicine.

REFERENCES

1. **Baba, T., S. Azuma, S. Kashiwabara, and Y. Toyoda.** 1994. Sperm from mice carrying a targeted mutation of the acrosin gene can penetrate the oocyte zona pellucida and effect fertilization. J. Biol. Chem. **269:**31845–31849.
2. **Baccetti, B.** 1979. The evolution of the acrosomal complex, p. 305–329. *In* D. W. Fawcett and J. M. Bedford (ed.), The spermatozoon. Urban & Schwarzenberg, Baltimore, MD.
3. **Bleil, J. D., J. M. Greve, and P. M. Wassarman.** 1988. Identification of a secondary sperm receptor in the mouse egg zona pellucida: role in maintenance of binding of acrosome-reacted sperm to eggs. Dev. Biol. **128:**376–385.
4. **Bleil, J. D., and P. M. Wassarman.** 1986. Autoradiographic visualization of the mouse egg's sperm receptor bound to sperm. J. Cell Biol. **102:**1363–1371.
5. **Bouchard, M. J., Y. Dong, B. M. McDermott, Jr., D. H. Lam, K. R. Brown, M. Shelanski, A. R. Bellve, and V. R. Racaniello.** 2000. Defects in nuclear and cytoskeletal morphology and mitochondrial localization in spermatozoa of mice lacking nectin-2, a component of cell-cell adherens junctions. Mol. Cell. Biol. **20:**2865–2873.
6. **Breed, W. G.** 2005. Evolution of the spermatozoon in muroid rodents. J. Morphol. **265:**271–290.
7. **Breed, W. G.** 2004. The spermatozoon of Eurasian murine rodents: its morphological diversity and evolution. J. Morphol. **261:**52–69.
8. **Castellani, L., F. Chiara, and F. Cotelli.** 1978. Fine structure and cytochemistry of the morphogenesis of round-headed human sperm. Arch. Androl. **1:**291–297.
9. **Cooper, T. G., and C. H. Yeung.** 2003. Acquisition of volume regulatory response of sperm upon maturation in the epididymis and the role of the cytoplasmic droplet. Microsc. Res. Tech. **61:**28–38.
10. **Coward, K., N. R. Bromage, O. Hibbitt, and J. Parrington.** 2002. Gamete physiology, fertilization and egg activation in teleost fish. Rev. Fish Biol. Fisheries **12:**33–58.
11. **Dam, A. H., I. Feenstra, J. R. Westphal, L. Ramos, R. J. van Golde, and J. A. Kremer.** 2007. Globozoospermia revisited. Hum. Reprod. Update **13:**63–75.
12. **Dean, J.** 2004. Reassessing the molecular biology of sperm-egg recognition with mouse genetics. Bioessays **26:**29–38.
13. **Eddy, E. M.** 2006. The spermatozoon, p. 3–54. *In* J. D. Neill (ed.), Knobil and Neill's physiology of reproduction, 3rd ed. Academic Press, Inc., San Diego, CA.
14. **Emanuelsson, O., S. Brunak, G. von Heijne, and H. Nielsen.** 2007. Locating proteins in the cell using TargetP, SignalP and related tools. Nat. Protoc. **2:**953–971.
15. **Florman, H. M., and T. Ducibella.** 2006. Fertilization in mammals, p. 55–112. *In* J. D. Neill (ed.), Knobil and Neill's physiology of reproduction, 3rd ed. Academic Press, Inc., San Diego, CA.
16. **Huang, T. T., Jr., and R. Yanagimachi.** 1985. Inner acrosomal membrane of mammalian spermatozoa: its properties and possible functions in fertilization. Am. J. Anat. **174:**249–268.
17. **Inagaki, M., K. Irie, H. Ishizaki, M. Tanaka-Okamoto, J. Miyoshi, and Y. Takai.** 2006. Role of cell adhesion molecule nectin-3 in spermatid development. Genes Cells **11:**1125–1132.
18. **Ito, C., F. Suzuki-Toyota, M. Maekawa, Y. Toyama, R. Yao, T. Noda, and K. Toshimori.** 2004. Failure to assemble the peri-nuclear structures in GOPC deficient spermatids as found in round-headed spermatozoa. Arch. Histol. Cytol. **67:**349–360.
19. **Katoh, M., and M. Katoh.** 2003. Identification and characterization of human ZPBP-like gene in silico. Int. J. Mol. Med. **12:**399–404.
20. **Kierszenbaum, A. L., E. Rivkin, and L. L. Tres.** 2003. Acroplaxome, an F-actin-keratin-containing plate, anchors the acrosome to the nucleus during shaping of the spermatid head. Mol. Biol. Cell **14:**4628–4640.
21. **Kierszenbaum, A. L., and L. L. Tres.** 2004. The acrosome-acroplaxome-manchette complex and the shaping of the spermatid head. Arch. Histol. Cytol. **67:**271–284.
22. **Kotaja, N., S. Kimmins, S. Brancorsini, D. Hentsch, J. L. Vonesch, I. Davidson, M. Parvinen, and P. Sassone-Corsi.** 2004. Preparation, isolation, and characterization of stage-specific spermatogenic cells for cellular and molecular analysis. Nat. Methods **1:**249–254.
23. **Letunic, I., R. R. Copley, B. Pils, S. Pinkert, J. Schultz, and P. Bork.** 2006. SMART 5: domains in the context of genomes and networks. Nucleic Acids Res. **34:**D257–D260.
24. **Lin, Y. N., and M. M. Matzuk.** 2005. High-throughput discovery of germ-cell-specific genes. Semin. Reprod. Med. **23:**201–212.
25. **Longo, F. J.** 1987. Fertilization. Chapman and Hall, New York, NY.
26. **Martianov, I., S. Brancorsini, R. Catena, A. Gansmuller, N. Kotaja, M. Parvinen, P. Sassone-Corsi, and I. Davidson.** 2005. Polar nuclear localization of H1T2, a histone H1 variant, required for spermatid elongation and DNA condensation during spermiogenesis. Proc. Natl. Acad. Sci. USA **102:**2808–2813.
27. **Matzuk, M. M., M. J. Finegold, J. G. Su, A. J. Hsueh, and A. Bradley.** 1992. Alpha-inhibin is a tumour-suppressor gene with gonadal specificity in mice. Nature **360:**313–319.
28. **Miller, B. J., E. Georges-Labouesse, P. Primakoff, and D. G. Myles.** 2000. Normal fertilization occurs with eggs lacking the integrin alpha6beta1 and is CD9-dependent. J. Cell Biol. **149:**1289–1296.
29. **Monne, M., L. Han, and L. Jovine.** 2006. Tracking down the ZP domain: from the mammalian zona pellucida to the molluscan vitelline envelope. Semin. Reprod. Med. **24:**204–216.
30. **Mori, E., T. Baba, A. Iwamatsu, and T. Mori.** 1993. Purification and characterization of a 38-kDa protein, sp38, with zona pellucida-binding property from porcine epididymal sperm. Biochem. Biophys. Res. Commun. **196:**196–202.
31. **Mori, E., S. Kashiwabara, T. Baba, Y. Inagaki, and T. Mori.** 1995. Amino acid sequences of porcine Sp38 and proacrosin required for binding to the zona pellucida. Dev. Biol. **168:**575–583.
32. **Morisawa, S.** 1999. Fine structure of micropylar region during late oogenesis in eggs of the hagfish *Eptatretus burgeri* (Agnatha). Dev. Growth Differ. **41:**611–618.
33. **Nagy, A.** 2003. Manipulating the mouse embryo: a laboratory manual, 3rd ed. Cold Spring Harbor Laboratory Press, Cold Spring Harbor, NY.
34. **Nakanishi, T., M. Ikawa, S. Yamada, M. Parvinen, T. Baba, Y. Nishimune,**

and M. Okabe. 1999. Real-time observation of acrosomal dispersal from mouse sperm using GFP as a marker protein. FEBS Lett. **449:**277–283.
35. **Ozaki-Kuroda, K., H. Nakanishi, H. Ohta, H. Tanaka, H. Kurihara, S. Mueller, K. Irie, W. Ikeda, T. Sakai, E. Wimmer, Y. Nishimune, and Y. Takai.** 2002. Nectin couples cell-cell adhesion and the actin scaffold at heterotypic testicular junctions. Curr. Biol. **12:**1145–1150.
36. **Primakoff, P., and D. G. Myles.** 2002. Penetration, adhesion, and fusion in mammalian sperm-egg interaction. Science **296:**2183–2185.
37. **Rajkovic, A., M. S. C. Yan, M. Klysik, and M. Matzuk.** 2001. Discovery of germ cell-specific transcripts by expressed sequence tag database analysis. Fertil. Steril. **76:**550–554.
38. **Roy, A., Y. N. Lin, and M. M. Matzuk.** 2007. Genetics of idiopathic male infertility, p. 99–111. *In* D. T. Carrell (ed.), The genetics of male infertility. Humana Press, Totowa, NJ.
39. **Roy, A., W. Yan, K. H. Burns, and M. M. Matzuk.** 2004. Tektin3 encodes an evolutionarily conserved putative testicular microtubules-related protein expressed preferentially in male germ cells. Mol. Reprod. Dev. **67:**295–302.
40. **Russell, L. D., R. A. Ettlin, S. Hikim, and E. D. Clegg.** 1990. Histological and histopathological evaluation of the testis. Cache River Press, St. Louis, MO.
41. **Smith, J., I. R. Paton, D. C. Hughes, and D. W. Burt.** 2005. Isolation and mapping the chicken zona pellucida genes: an insight into the evolution of orthologous genes in different species. Mol. Reprod. Dev. **70:**133–145.
42. **Stein, K. K., J. C. Go, W. S. Lane, P. Primakoff, and D. G. Myles.** 2006. Proteomic analysis of sperm regions that mediate sperm-egg interactions. Proteomics **6:**3533–3543.
43. **Suzuki-Toyota, F., C. Ito, Y. Toyama, M. Maekawa, R. Yao, T. Noda, and K. Toshimori.** 2004. The coiled tail of the round-headed spermatozoa appears during epididymal passage in GOPC-deficient mice. Arch. Histol. Cytol. **67:**361–371.
44. **Tanii, I., K. Yoshinaga, and K. Toshimori.** 1999. Morphogenesis of the acrosome during the final steps of rat spermiogenesis with special reference to tubulobulbar complexes. Anat. Rec. **256:**195–201.
45. **Vogl, A. W., D. C. Pfeiffer, D. Mulholland, G. Kimel, and J. Guttman.** 2000. Unique and multifunctional adhesion junctions in the testis: ectoplasmic specializations. Arch. Histol. Cytol. **63:**1–15.
46. **Williams, Z., E. S. Litscher, L. Jovine, and P. M. Wassarman.** 2006. Polypeptide encoded by mouse ZP3 exon-7 is necessary and sufficient for binding of mouse sperm in vitro. J. Cell Physiol. **207:**30–39.
47. **Yan, H. H., D. D. Mruk, W. M. Lee, and C. Y. Cheng.** 2007. Ectoplasmic specialization: a friend or a foe of spermatogenesis? Bioessays **29:**36–48.
48. **Yan, W., A. Rajkovic, M. M. Viveiros, K. H. Burns, J. J. Eppig, and M. M. Matzuk.** 2002. Identification of Gasz, an evolutionarily conserved gene expressed exclusively in germ cells and encoding a protein with four ankyrin repeats, a sterile-alpha motif, and a basic leucine zipper. Mol. Endocrinol. **16:**1168–1184.
49. **Yanagimachi, R.** 1994. Mammalian fertilization, p. 189–317. *In* E. Knobil and J. D. Neill (ed.), The physiology of reproduction, vol. 1. Raven Press, New York, NY.
50. **Yao, R., C. Ito, Y. Natsume, Y. Sugitani, H. Yamanaka, S. Kuretake, K. Yanagida, A. Sato, K. Toshimori, and T. Noda.** 2002. Lack of acrosome formation in mice lacking a Golgi protein, GOPC. Proc. Natl. Acad. Sci. USA **99:**11211–11216.
51. **Yu, Y., W. Xu, Y. J. Yi, P. Sutovsky, and R. Oko.** 2006. The extracellular protein coat of the inner acrosomal membrane is involved in zona pellucida binding and penetration during fertilization: characterization of its most prominent polypeptide (IAM38). Dev. Biol. **290:**32–43.